ACS BIO & MED CHEM Au
AN OPEN ACCESS JOURNAL OF THE AMERICAN CHEMICAL SOCIETY

pubs.acs.org/biomedchemau

Article

Sex-Specific Silica Nanoparticle Protein Corona Compositions Exposed to Male and Female BALB/c Mice Plasmas

Ali Akbar Ashkarran,[○] Hassan Gharibi,[○] Jason W. Grunberger, Amir Ata Saei,* Nitish Khurana, Raziye Mohammadpour, Hamidreza Ghandehari, and Morteza Mahmoudi*

Cite This: *ACS Bio Med Chem Au* 2023, 3, 62–73

Read Online

ACCESS | Metrics & More | Article Recommendations | Supporting Information

ABSTRACT: As various nanoparticles (NPs) are increasingly being used in nanomedicine products for more effective and less toxic therapy and diagnosis of diseases, there is a growing need to understand their biological fate in different sexes. Herein, we report a proof-of-concept result of sex-specific protein corona compositions on the surface of silica NPs as a function of their size and porosity upon incubation with plasma proteins of female and male BALB/c mice. Our results demonstrate substantial differences between male and female protein corona profiles on the surface of silica nanoparticles. By comparing protein abundances between male and female protein coronas of mesoporous silica nanoparticles and Stöber silica nanoparticles of ∼100, 50, and 100 nm in diameter, respectively, we detected 17, 4, and 4 distinct proteins, respectively, that were found at significantly different concentrations for these constructs. These initial findings demonstrate that animal sex can influence protein corona formation on silica NPs as a function of the physicochemical properties. A more thorough consideration of the role of plasma sex would enable nanomedicine community to design and develop safer and more efficient diagnostic and therapeutic nanomedicine products for both sexes.

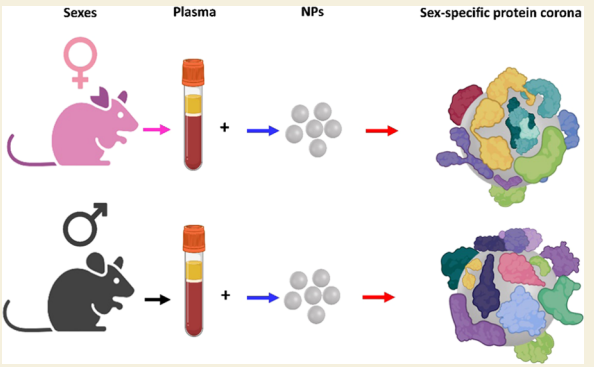

KEYWORDS: *plasma sex, protein corona, biological identity, nanomedicine, nanodiagnostics, nanotherapeutics*

INTRODUCTION

Nanoparticle-based drug delivery has yet to markedly increase the overall survival rates of diseases such as cancer beyond conventional parent drugs.[1,2] This reflects the insufficient understanding of NP interaction with biointerfaces, including how the patient biological variables such as sex influence the dosage and therapeutic efficacy. Highly successful monoclonal antibodies failed their first decade of clinical trials because murine monoclonals were being tested in humans and only with humanized/human monoclonals did clinical trials succeed.[3] The works of our team[4,5] and others[1] suggest that nanomedicines follow a similar track; the clinical development of NPs will lag until factors critical to their therapeutic efficacy are fully identified and characterized.[6,7]

Among numerous biological variables, sex critically influences disease occurrence and progression.[8] In cancer, for example, tumor incidence, growth, cellular−molecular phenotypes, and therapeutic efficacies are sex-linked.[9−11] Sex differences related to genetic variations include the abnormal reactivation of X-linked genes,[12] differences in deletion/duplication of segments on X/Y chromosomes,[10] mutated genes in tumors,[13] transcription factor patterns,[11] and the sex-specific roles of hormones.[14−17] Despite the significant effect of sex on NPs,[18] its effects on the therapeutic and diagnostic functions of NPs are not fully explored. While other biological barriers such as neovasculature disruption, treatment history, and other underlying health states can also affect the therapeutic and diagnostic efficacy of nanomedicines, this research focuses on sex differences as a profound, yet overlooked factor in preclinical studies. It is well documented that medication and treatment are different for male and female individuals due to their differences in many aspects (e.g., metabolism).[19] For example, it is reported that cell sex significantly influences the cellular uptake of NPs. It is found that cells from men and women respond differently to reprogramming techniques used to enhance the ability of the cells to differentiate into a greater variety of cell types.[20]

Once exposed to biological fluids, the surface of most NPs is rapidly covered with ions and biomolecules; this corona determines the biological fate of NPs.[21,22] Studies, however, have largely overlooked the significant impact of protein corona on NP function in both *in vitro* and *in vivo* microenvironments. Such negligence has often led to

Received: June 13, 2022
Revised: October 21, 2022
Accepted: October 21, 2022
Published: November 7, 2022

https://doi.org/10.1021/acsbiomedchemau.2c00040
ACS Bio Med Chem Au 2023, 3, 62–73

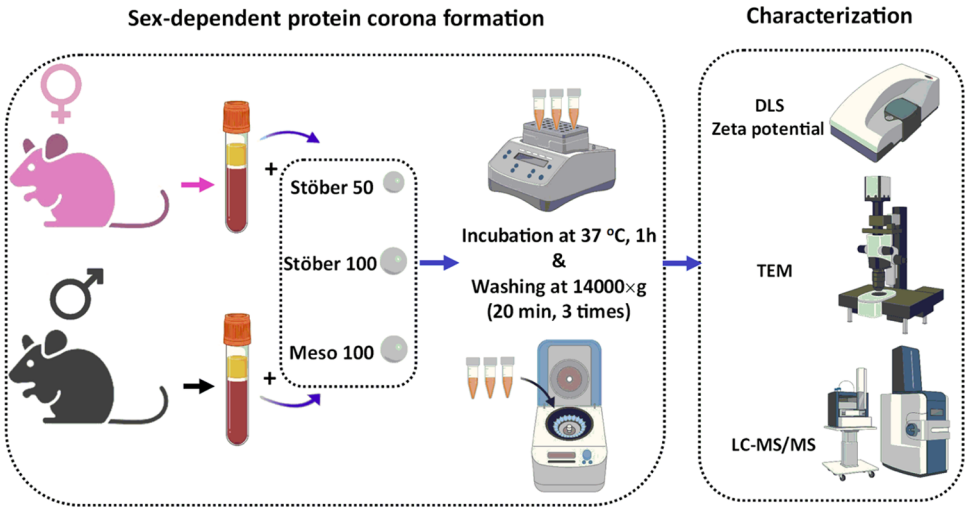

Figure 1. Schematic workflow for the generation of the sex-specific protein coronas on three different types of NPs. NPs with and without protein corona were physicochemically characterized by dynamic light scattering (DLS), ζ-potential analysis, and transmission electron microscopy (TEM). The formed protein coronas were profiled by liquid chromatography coupled to mass spectrometry (LC-MS/MS) to investigate sex-specific differences in protein coronas.

inaccurate predictions of NPs' fate, safety, and therapeutic efficacy in both animal models and human subjects.[1,23] We recently reviewed the corrective efforts made to address this gap,[24,25] which have mainly centered on (1) identifying overlooked/unknown factors in the NP microenvironment; (2) improving NP toxicity assays; (3) optimizing the *in vitro* protocols to better mimic *in vivo* conditions; and (4) combining electron microscopy and computational approaches to mechanistically understand protein corona.[23,26,27]

Plasma proteome[28] and metabolome[29] profiles differ substantially between sexes. One study, for example, found 231 proteins with significant differences in abundance between sexes.[28] We also reported variations in the proteomic[30,31] and metabolomic[30,32] compositions of plasma substantially affecting the NP protein corona profile. The biomolecular corona including lipids, metabolomes, proteins, and other biomolecules alters the original surface of the NPs and gives them a new biological identity after exposure to biological fluids, and most studies in nanomedicine have not properly considered such crucial biological variables *in vitro* and *in vivo* microenvironments.[33] In fact, metabolome profiles of males and females are significantly different due to substantial differences in their corresponding amino acids, fatty acids, and lipid profiles.[34] Since the metabolome profile can significantly affect the interactions of nanomaterials and biological fluid, we may expect metabolomics variations to affect the protein corona composition of NPs in a sex-specific manner.[35] Thus, sex-based differences in plasma composition can induce major variations in NP protein corona, consequently affecting its diagnostic and therapeutic efficacies.

While biological interactions with NPs have been widely investigated,[23,36] a few studies have examined the influence of sex.[35] We recently reported on how sex alters NP uptake and intracellular trafficking in human amniotic mesenchymal stem cells, cancer cells, and leukocytes.[20,37] Furthermore, it has been reported that toxic silver NPs significantly alter the bacterial species harbored in male zebrafish but not in females.[38]

In this study, we selected silica NPs with variations in porosity and size, previously studied for their chronic toxicity,[39−41] and probed their sex-specific protein corona compositions. Silica and silica-based multimodal nanostructures with different sizes and various unique properties have been widely used for therapeutic and diagnostic applications mainly through the delivery of drugs, genes, and contrast agents.[42,43] We selected silica as a model NP due to its safety and promising wide range of applications in therapeutic nanomedicine.[44−46] In addition, silica NPs have been widely used for protein corona studies by various groups.[47−51]

EXPERIMENTAL DETAILS

Materials

Silica Nanoparticle Synthesis. Three silica NPs (i.e., Stöber 50, Stöber 100, and mesoporous 100) were synthesized. Stöber 100 was prepared as follows: 1700 mmol of absolute ethanol, 155 mmol of deionized water, and 26 mmol of ammonium hydroxide were mixed in a 250 mL Erlenmeyer flask under a stirring rate of 400 rpm for 10 min. Then, 16 mmol of TEOS was added dropwise and the reaction was left stirring for 24 h at room temperature. The synthesized particles were collected by centrifugation using an Avanti J-15R (Beckman Coulter Inc., Indianapolis, IN) at 11 420*g* for 10 min and washed thrice with water and 95% ethanol. Stöber 50 particles were prepared as follows: 15.4 mol of absolute ethanol, 1.4 mol of deionized water, and 0.16 mol of ammonium hydroxide were mixed in a 2000 mL round-bottom flask under a stirring rate of 500 rpm for 10 min. Then, 0.15 mol of TEOS was added dropwise and the reaction was left stirring for 24 h at room temperature. The synthesized particles were collected by centrifugation and washed thrice with water and 95% ethanol. Mesoporous 100 was prepared as follows: 6600 mmol of deionized water, 1.7 mmol of sodium hydroxide, and 0.7 mmol of CTAB were mixed in a 250 mL round-bottom flask under a stirring rate of 300 rpm for 1 h at 80 °C. Then, the stirring rate was increased to 800 rpm and 5.4 mmol of TEOS was added dropwise. After 2 h, the reaction was cooled and the synthesized particles were collected by centrifugation and washed thrice with water and 95% ethanol. Lastly, the CTAB was extracted with an acidic ethanol wash (1 mL of concentrated HCl in 30 mL of absolute ethanol) at 80 °C under reflux for 6 h. The particles were collected by centrifugation and washed thrice with water and 95% ethanol. All particles were stored in DI water, where the final mass concentration was determined.

Silica Nanoparticle Characterization. Transmission electron microscopy (TEM) images were acquired by a JEOL JEM-1400 Plus transmission electron microscope (Peabody, MA) operating at 120

https://doi.org/10.1021/acsbiomedchemau.2c00040
ACS Bio Med Chem Au 2023, 3, 62−73

Table 1. Average Size, Polydispersity Index (PDI), ζ-Potential, and the Corresponding Standard Deviation (SD) Values of Bare NPs and Male and Female Protein Corona-Coated NPs[a]

	before protein corona			after protein corona					
nanoparticle	Stöber 50	Stöber 100	mesoporous 100	Stöber 50-M	Stöber 50-F	Stöber 100-M	Stöber 100-F	mesoporous 100-M	mesoporous 100-F
size (nm)	48.4	98.7	105.7	56.0	62.2	135.3	103.1	108.7	122.4
SD (nm)	3.9	0.3	0.0	4.6	9.9	11.2	4.4	12.5	0.0
PDI	0.091	0.048	0.147	0.193	0.38	0.117	0.142	0.183	0.236
ζ-potential (mV)	−15.0	−14.3	−10.5	−14.6	−10.0	−9.2	−10.3	−14.3	−11.3
SD (mV)	0.6	1.6	0.9	3.0	1.9	0.4	3.6	3.6	1.9

[a]M: male and F: female; three technical repeats.

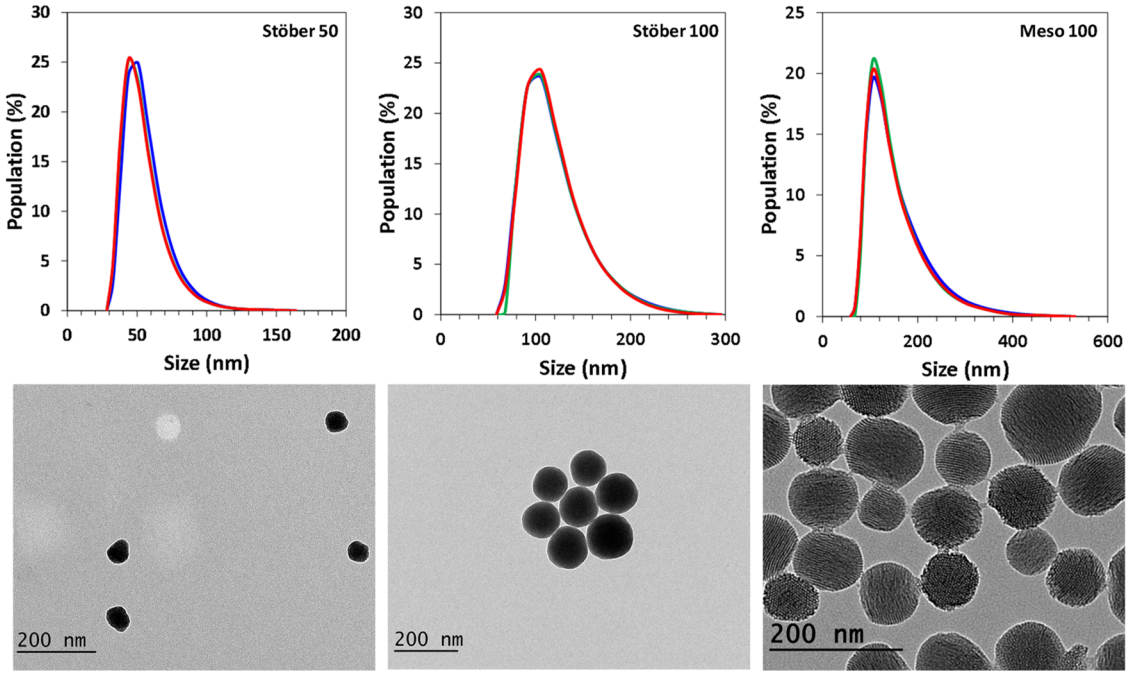

Figure 2. Size distribution and microscopic characterization of bare NPs before protein corona formation. DLS plots (top panel) of 200 μg/mL of bare NPs in PBS (three technical repeats) and the corresponding TEM images of the same NPs (bottom panel).

kV. Formvar-coated carbon TEM grids were prepared by drop-casting nanoparticles suspended in 95% ethanol and dried at room temperature.

Plasma Isolation. Six female and male BALB/c mice (43−49 days old) were purchased from Charles River Laboratories (strain code #082). All mice were acclimated in the animal facility for 2 weeks prior to blood collection and were maintained under 22−24 °C and 20% humidity, subjected to a 12 h light/dark cycle with free access to food (2029X) and water. All procedures were approved by the University of Utah Institutional Animal Care and Use Committee (IACUC). Blood was withdrawn from the hearts of mice under anesthesia using 31G needle syringes. The collected blood was added to EDTA-coated BD Vacutainer blood collection tubes (Mississauga, ON, Canada) and stored on ice. Within 2 h of blood collection, plasma was obtained by centrifugation of blood samples at 3000 rpm for 15 min at 4 °C and frozen at −80 °C until they were ready for use. The obtained plasmas from each sex (n = 3) were pooled to minimize the effect of personalized protein corona signals on the corona compositions. The male and female BALB/c mice plasmas were diluted with phosphate buffer solution (PBS, 1×) to a concentration of 55%.

Protein Corona Formation on the Surface of the NPs. For protein corona formation, each NP type was incubated with 55% sex-specific plasmas (with NP concentration of 200 μg/mL) for 1 h at 37 °C. To remove unbound and loosely attached plasma proteins to the surface of NPs, the protein−NP complexes were then centrifuged at 14 000g for 20 min; the collected NPs' pellets were washed two more times with cold PBS under the same conditions. The final pellet was redispersed in 100 μL of PBS and used for further analysis (Figure 1).

Physicochemical Characterization. Dynamic light scattering (DLS) and ζ-potential analyses were performed to measure the size distribution and ζ-potential of the NPs before and after protein corona formation using a Zetasizer nano series DLS instrument (Malvern Panalytical). A helium−neon laser with a wavelength of 632 nm was used for the size distribution measurement at room temperature. TEM of corona-coated nanoparticles was carried out using a JEM-2200FS (JEOL Ltd.) operated at 200 kV. The instrument was equipped with an in-column energy filter and an Oxford X-ray energy-dispersive spectroscopy (EDS) system. 20 μL of the bare and protein corona-coated NPs were drop-casted onto a copper grid followed by negative staining using 20 μL of 1% uranyl acetate and finally washed with DI water and used for imaging on the same day. Protein corona profiles of NPs exposed to male and female mice plasma NPs were studied by sodium dodecyl sulfate-polyacrylamide gel electrophoresis (SDS-PAGE) analysis.

Proteomics Sample Preparation. Each sample was buffered by adding triethylammonium bicarbonate buffer (TEAB, Honeywell Fluka cat# 60-044-974) to a final concentration of 20 mM. Samples were reduced by adding 5 mM DL-dithiothreitol (DTT, Sigma-Aldrich cat# D5545) and incubated for 30 min at 37 °C. Alkylation was performed by adding 15 mM of iodoacetamide (IAA, Sigma-Aldrich cat# I1149) and incubating samples at room temperature for 30 min

https://doi.org/10.1021/acsbiomedchemau.2c00040
ACS Bio Med Chem Au 2023, 3, 62−73

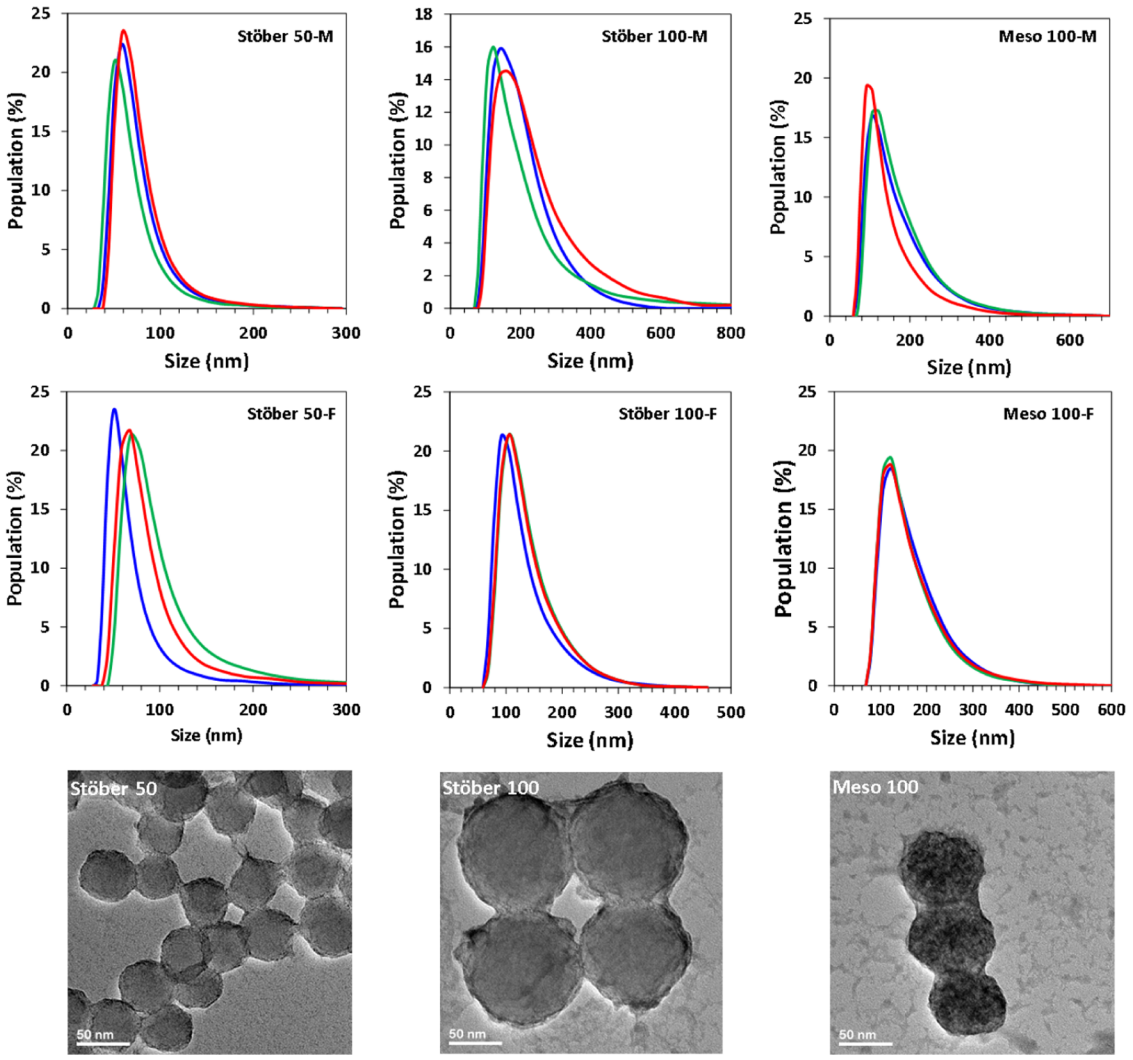

Figure 3. DLS plots of male (-M) and female (-F) protein corona-coated NPs (three technical repeats) and the corresponding TEM images of NPs coated with male plasma proteins, as representative examples (TEM images of female protein corona-coated sample were similar to that of male and are presented in Figure S1).

in the dark. The alkylation reaction was stopped by adding 5 mM of DTT to the samples. The tryptic digest was initiated by adding 0.35 μg of trypsin (Promega, V5113) per tube and then incubating 1 h at 47 °C followed by 3 h at 37 °C. Digestion was assessed by running a small aliquot of each sample on LC-MS/MS.

LC-MS/MS. LC-MS/MS was performed using data-dependent analysis. MS1 spectra were acquired at 120 000 resolution and MS2 in the ion trap. Digested samples were dried and then solubilized in mobile phase A (0.1% formic acid) and then analyzed using an Easy nLC 1000 coupled to an Orbitrap Fusion mass spectrometer (Thermo Fisher Scientific). The injection volume was set at 16 μL for a 1.0 μg sample. Digests were loaded onto a PepMap 100 C18 trap column, 75 μm id × 2 cm length (Thermo Fisher Scientific) at 3 μL/min for 10 min with mobile phase A as the carrier, followed by separation on an Acclaim PepMap RSLC 2 μm C18 column, 75 μm id × 25 cm length (Thermo Fisher Scientific) at 45 °C. Peptides were separated using a 90 min four-step gradient of 5−11% B over 25 min, 11−18% B over 25 min, 18−28% B over 24 min, 28−42% B over 5 min and finishing with 100% mobile phase B (100% acetonitrile with 0.10% formic acid) for 11 min. All steps were carried out at a flow rate of 250 nL/min. The Orbitrap Fusion was operated with positive polarity in data-dependent acquisition (DDA) mode at a spray voltage of 1900 V, and the ion transfer tube was heated to 275 °C. The 445.1200 ion was used as a lock mass. The full scan resolution was set at 120 000, the mass range was 350−1600 m/z, the RF lens was set at 60%, the full scan ion target value was 4.0×10^5 allowing a maximum injection time of 75 ms, and data were collected in the profile mode. Ions with charge states 2−7 were accepted for MS2 spectra, which were collected in the ion trap. Ions were excluded for 60 s after 1 acquisition. Quadrupole isolation was used with a 1.6 Da isolation window. The collision energy was fixed at CID = 29 with a 10 ms activation time and 0.25 activation Q. The scan rate was set to a rapid mode with a maximum injection time of 75 ms and an AGC target of 10 000. MS2 data were centroided.

Proteomics Data Extraction and Processing. Data were analyzed using Proteome Discoverer 2.4 using Sequest NT and Percolator algorithms, searching a Mouse database downloaded on March 30th, 2021 (Uniprot UP000000589) with 17 035 protein entries. Parameters in the search were set to accept up to two missed cleavages by trypsin digestion. Carbamidomethylation of cysteine was a fixed modification, and dynamic modifications were deamination of asparagine and glutamine as well as oxidation of methionine. An additional dynamic N-terminus acetyl modification was also applied. A false discovery rate (FDR) was set at 0.01 for high confidence matches. Protein abundances were normalized by the total protein abundance in each replicate. Only proteins with at least two peptides (and at least one unique peptide) were included in the final data set, and all of the contaminants were removed. Fold changes were calculated as the normalized abundance of a given protein in male vs female coronas.

https://doi.org/10.1021/acsbiomedchemau.2c00040
ACS Bio Med Chem Au 2023, 3, 62−73

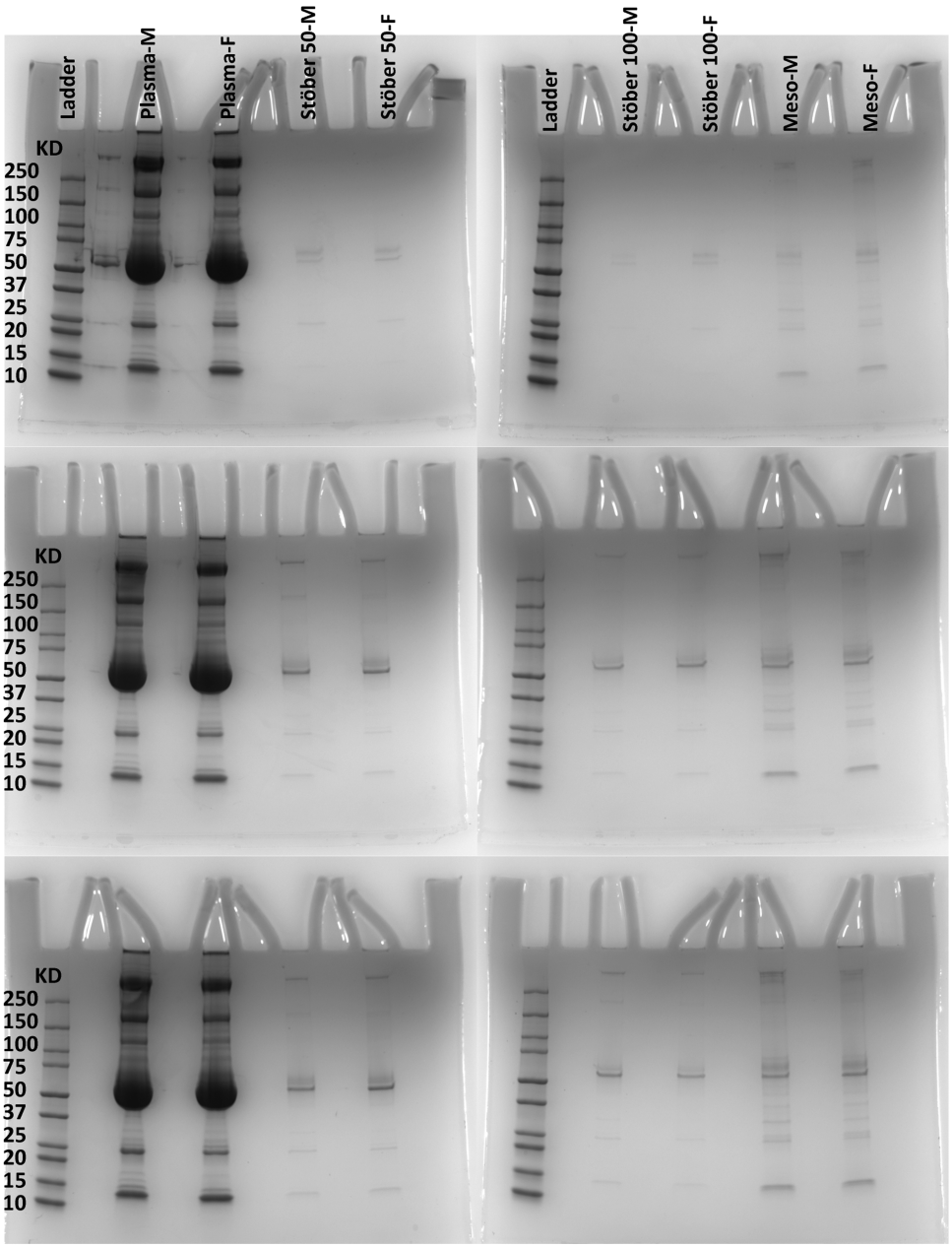

Figure 4. SDS-PAGE results of male and female protein corona-coated NPs (from top to bottom are three technical repeats of the same samples, respectively) show that protein corona profiles (band intensities) are sex-dependent in different sexes to some extent.

RESULTS AND DISCUSSION

Prior to the formation of protein corona, the bare NPs were analyzed by DLS and TEM to characterize the size, size distribution, and surface charge of the particles (Table 1). Figure 2 also demonstrates the size distribution histograms (three technical repeats) of different NPs used in this study and the corresponding TEM images.

Table 1 also demonstrates the summary of the average size and ζ-potential values of sex-specific protein corona-coated NPs in addition to the bare NPs. Figure 3 shows the size distribution (three technical repeats) histograms as well as the TEM images of male and female protein corona-coated NPs. It is noteworthy that the SD presented in Table 1 refers to the SD of the mean particle size (calculated from three technical replicates) and not the SD of whole size distribution. As expected, the average diameter of all NPs was increased from ~8 to 35 nm in some NPs due to the formation of protein corona on the surface of the NPs. Although in general the sizes of plasma proteins vary between 1 and 10 nm, there may be protein−protein interactions, agglomeration of NPs due to the formation of protein corona and viscosity of the proteins, and many other possible interactions of protein corona-coated NPs, which may increase the average size of the protein-coated NPs more than 10 nm. In fact, due to different protein corona compositions of male and female protein corona-coated NPs and their corresponding interactions, we may see large variations in the size of the protein corona-coated NPs. In addition, the formation of protein corona is further confirmed by alteration of the surface charge of the NPs (Table 1).

TEM analysis was also used to qualitatively investigate the size of the NPs after the formation of the protein corona. Protein corona-coated NPs were stained using 1% uranyl

https://doi.org/10.1021/acsbiomedchemau.2c00040
ACS Bio Med Chem Au 2023, 3, 62−73

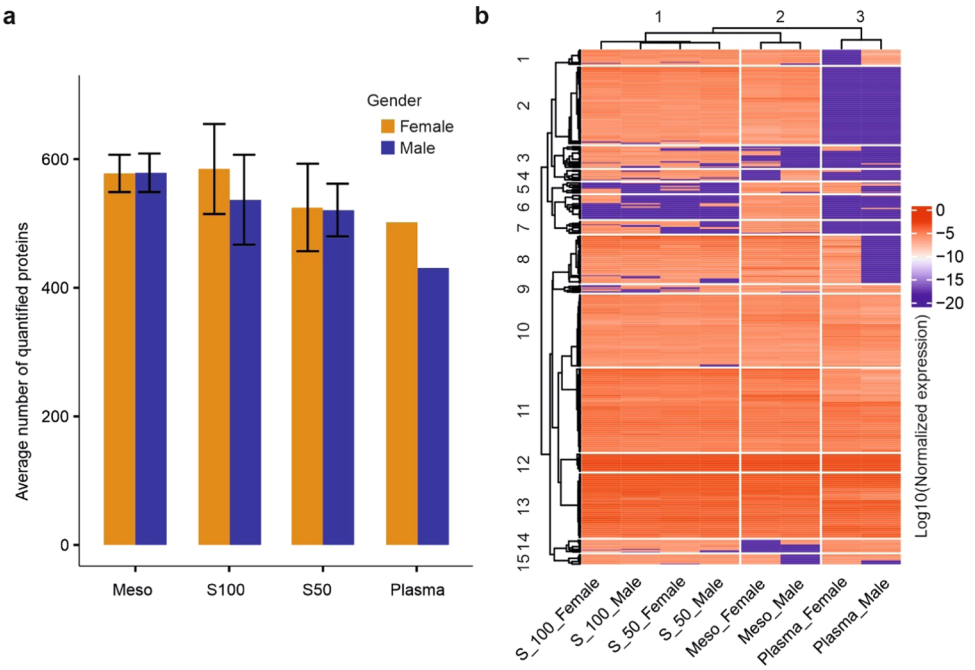

Figure 5. (a) Average number of proteins quantified for each type of NP corona, and (b) the hierarchical clustering of samples based on the average abundances of quantified proteins in male and female whole plasmas and various protein coronas (meso, S100, and S50 refer to mesoporous, Stöber 100, and Stöber 50, respectively).

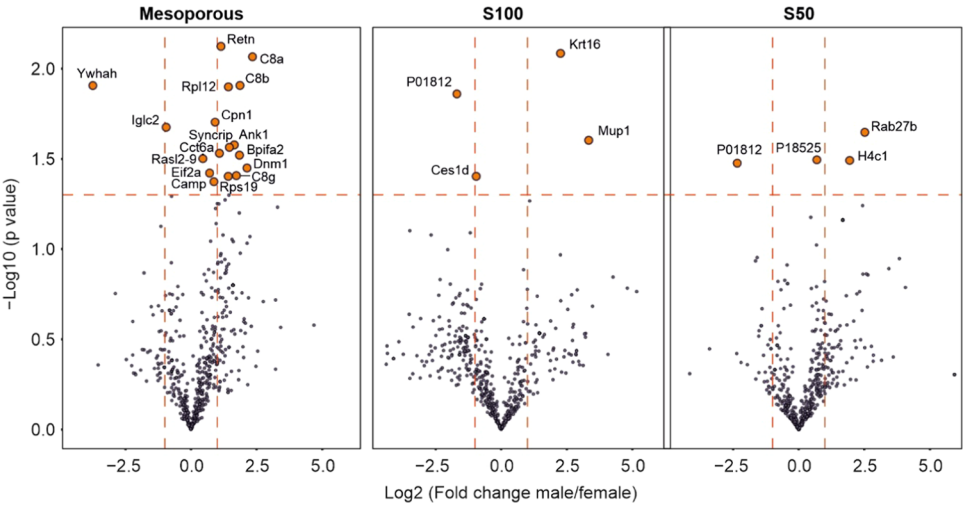

Figure 6. Comparison of fold changes of proteins in coronas of three different silica NPs (S100 and S50 refer to Stöber 100 and Stöber 50, respectively) after incubation with male vs female plasma (two-sided Student's *t*-test).

acetate to increase the contrast of the corona layer around the NPs (Figure 3). TEM images of the protein corona-coated NPs confirm that a very thin dark layer surrounded NPs, indicating that NPs are randomly coated with protein corona.[22,52]

As a next step, we analyzed the composition of the male and female protein coronas on the surface of various NPs using the one-dimensional (1D) SDS-PAGE analysis (Figure 4). Considering the resolution of the 1D SDS-PAGE, the protein corona profiles of male and female plasmas did not show significant visual differences. Therefore, we performed LC-MS/MS analysis on the male and female protein corona profiles of various NPs.

The LC-MS/MS outcomes of the male and female protein coronas at the surface of various NPs together with the male and female whole plasma analysis resulted in the identification of 1690 proteins (Table S1). The total average number of quantified proteins in each sample type is shown in Figure 5a. The number of proteins quantified were slightly higher for female vs male in most cases. Furthermore, a relatively higher number of proteins were quantified in protein coronas compared to those of plasma. This effect can be attributed to the enrichment of a specific set of proteins and reduction of proteome dynamic range by NPs, leading to the detection of more proteins, which can be advantageous in biomarker discovery.[53,54]

The protein intensities were normalized to the total protein intensity in each sample and were then log 10-transformed. For normalization across all samples, the values for missing proteins in each sample were set to 10^{-20}. The average relative

https://doi.org/10.1021/acsbiomedchemau.2c00040
ACS Bio Med Chem Au 2023, 3, 62−73

Table 2. Proteins with Significant Changes in the Protein Corona of Different NPs in Male vs Female Coronas

NP type	gene name	protein name	log 2 fold change in male vs female corona	*P* value
mesoporous 100	Retn	resistin	1.18	0.008
	C8a	complement component C8 α chain	2.38	0.009
	C8b	complement component C8 β chain	1.89	0.012
	Ywhah	14-3-3 protein eta	−3.71	0.012
	Rpl12	60S ribosomal protein L12	1.46	0.013
	Cpn1	carboxypeptidase N catalytic chain	0.96	0.020
	Iglc2	Ig lambda-2 chain C region	−0.91	0.021
	Ank1	Ankyrin-1	1.69	0.026
	Syncrip	heterogeneous nuclear ribonucleoprotein Q	1.49	0.027
	Cct6a	T-complex protein 1 subunit zeta	1.11	0.029
	Bpifa2	BPI fold-containing family A member 2	1.87	0.030
	Rasl2	GTP-binding nuclear protein Ran, testis-specific isoform	0.49	0.030
	Dnm1	Dynamin-1	2.16	0.036
	Eif2a	eukaryotic translation initiation factor 2A	0.75	0.038
	C8g	complement component C8 γ chain	1.76	0.039
	Rps19	40S ribosomal protein S19	1.45	0.040
	Camp	cathelicidin antimicrobial peptide	0.91	0.042
Stöber 100	keratin, type I cytoskeletal 16	Krt16	2.30	0.008
	Ig heavy-chain V region MOPC 173		−1.66	0.014
	major urinary protein 1	Mup1	3.37	0.025
	carboxylesterase 1D	Ces1d	−0.91	0.040
Stöber 50	Ras-related protein Rab27B	Rab27b	2.56	0.023
	Ig heavy-chain V region 5−84		0.72	0.032
	histone H4	H4c1	1.98	0.032
	Ig heavy-chain V region MOPC 173		−2.31	0.033

abundances of three technical replicates for each sample type were plotted through hierarchical clustering in Figure 5b. Proteins in each cluster are listed in Table S2. Proteins in clusters 10−13 were almost consistently quantified in all samples, while the other clusters were quantified with high variability depending on the type of NPs or in whole plasma.

To identify significant sex-specific protein features in the protein corona profiles of NPs, we compared protein abundances in the corona of plasma from male vs female mice for each NP type (Figure 6). A total of 25 proteins (17, 4, and 4 distinct proteins between male and female protein coronas of mesoporous silica nanoparticles and Stöber silica nanoparticles of ∼100, 50, and 100 nm in diameter, respectively) were identified with significant differences (P value <0.05) in male vs female (or vice versa) protein corona profiles of the three NP types (Table S3). In general, while a lower number of proteins were quantified in whole male plasma or male coronas compared to female counterparts, there were more outliers with significantly higher concentrations in the male coronas. This is mainly because of the fact that the protein corona profile of plasma has a poor correlation, in amount or type, with proteins in plasma (i.e., the most abundant proteins in plasma, such as albumin, make limited contributions to the corona layer); this corona's unique feature overcomes several problems in the global discovery of plasma proteomics, including the adverse effects of highly abundant proteins, which impede the robust detection of low-abundance proteins;[55,56] i.e., using NP arrays, one can capture a higher number of proteins in their coronas.

Of the identified 25 proteins with significant differences between male and female plasmas, 7 were not quantified in whole male or female plasma and an additional one was not quantified in whole male plasma, showing that NP corona allows for the deep sampling of plasma and eventually quantification of more proteins, as shown before.[31,53,54]

Comparing protein abundances between male and female protein coronas of mesoporous 100 NPs, 17 proteins were found at significantly higher concentrations in either male or female coronas (Table 2).

Out of these, eight proteins were related to the immune system process, namely, complement component 8 (C8a, C8b, and C8g), immunoglobulin lambda constant 2 (Iglc2), synaptotagmin-binding, cytoplasmic RNA-interacting protein (Syncrip), ankyrin-1 (Ank1), catabolite activator protein (Camp), and ribosomal protein S19 (Rps19). We subjected the 17 significant proteins to pathway enrichment analysis in StringDB and identified several enriched biological processes, especially those involved in immune processes, shown in Table 3.

Interestingly, KEGG analysis also revealed the enrichment of "systemic lupus erythematosus" and "amoebiasis" (3 proteins, $P = 0.0167$), showing the capacity of protein corona profiles in identifying important disease-related proteins.

Among the 17 significant proteins, 15 were found at greater concentrations in the male vs female coronas. The top protein with higher concentrations in male coronas was Retn or resistin, which is a hormone known to suppress the ability of insulin in stimulating glucose uptake into adipocytes and is also known to be involved in inflammation.[57,58] Interestingly, several studies have already shown that resistin signaling is sex-dependent.[58,59] Resistin is a protein with high diagnostic potential. Resistin response is implicated in the onset of obesity with sex-associated differences in rats and potentially links obesity to diabetes.[60] This adipokine could potentially serve as one of the metabolic signals that partially explain infertility related to obesity, for example, those resulting from

https://doi.org/10.1021/acsbiomedchemau.2c00040
ACS Bio Med Chem Au 2023, 3, 62−73

Table 3. Enriched Biological Pathways for 17 Proteins with Significant Differences in Male vs Female Coronas of Mesoporous NPs

GO term	biological process	number of proteins	strength	*P* value
GO:0006957	complement activation, alternative pathway	3	2.59	0.0002
GO:0019835	cytolysis	4	2.33	5.38×10^{-5}
GO:0006958	complement activation, classical pathway	4	2.20	6.74×10^{-5}
GO:0006959	humoral immune response	6	1.66	5.38×10^{-5}
GO:0042742	defense response to bacterium	4	1.30	0.0209
GO:0050778	positive regulation of immune response	5	1.16	0.0113
GO:0045087	innate immune response	6	1.14	0.0023
GO:0098542	defense response to other organisms	8	1.13	0.0001
GO:0006955	immune response	7	0.97	0.0035
GO:0002376	immune system process	8	0.75	0.0151
GO:0009605	response to external stimulus	9	0.72	0.0073
GO:0048518	positive regulation of biological process	13	0.46	0.0140
GO:0050896	response to stimulus	14	0.42	0.0120

polycystic ovary syndrome (PCOS).[58] This finding validates our methodology coupled to LC-MS analysis in the detection of sex-specific differences in NP coronas of male vs female. In addition, due to the essential roles of resistin in inflammation and signaling, in humans, this protein is emerging as a biomarker for various diseases including inflammatory bowel disease,[61] colorectal cancer,[62] atherosclerosis,[63] ischemic heart disease,[63,64] hypertension,[65] and rheumatoid arthritis,[66] among others. Other top proteins that could serve as diagnostic or prognostic biomarkers in humans include Cpn1 or carboxypeptidase N catalytic chain for breast cancer,[67] Cct6a or T-complex protein 1 subunit zeta for hepatocellular carcinoma,[68] Ewing sarcoma,[68] and BPI fold-containing family A member 2 or Bpifa2 in acute kidney injury.[69] Finally, Camp is cathelicidin antimicrobial peptide that exerts an antibacterial activity by binding to bacterial lipopolysaccharides (LPS) and is clinically relevant. For example, the low plasma level of this peptide predicts increased infectious disease mortality in patients undergoing hemodialysis.[70]

Among the identified top 17 proteins, three complement factors including C8a, C8b, and C8g (complement component C8 α, β, and γ chain precursor proteins) were standing out in male coronas vs females. These proteins constitute the membrane attack complex (MAC) that is essential for innate and adaptive immune responses by forming pores in the plasma membrane of target cells.[71] There is increasing evidence that the complement protein (e.g., C8) levels responsible for immune responses are critically different between sexes.[72,73] It is reported that proteins involved in IL-4 and IL-6 signaling, complement activation, and blood coagulation disorders show different and opposing changes among stroke patients of different sexes.[74] It is also shown that sex chromosome complement contributes to sex-based differences in susceptibility to autoimmune encephalomyelitis and lupus. A significant difference was observed in Th2 cytokines (i.e., IL-13, -4, and -10) production, with higher levels from cells derived from XY^- mice.[75]

On the other hand, two proteins Ywhah and Iglc2 had a higher abundance in female coronas compared to their male counterparts. Ywhah or 14-3-3 protein eta is an adapter protein that can bind to a large number of other proteins through the recognition of phosphoserine or phosphothreonine motif. Since Ywhah binding generally modulates the activity of the binding protein, this protein is involved in the regulation of a large number of general and specialized signaling pathways. In humans, YWHAH might be associated with various cancers, and its polymorphisms are implicated to be genetically associated with schizophrenia.[76] In humans, Iglc2 or (Ig lambda-2 chain C region) gene has been recently linked to the prognosis of triple-negative breast cancer[77] and its deposition in AL-amyloid lesions is linked to a new disease entity of AL amyloidosis.

Comparing protein abundances between male and female protein coronas of Stöber 100 NPs, 4 proteins had a *P* value <0.05 (major urinary protein 1 or Mup1, keratin, type I cytoskeletal 16 or Krt16, Ig heavy-chain V region MOPC 173, and carboxylesterase 1D or Ces1d) (Table 2). Mup1 (sometimes called male urinary protein) is abundant in the urine of adult male mice but was believed to be absent from that of females; however, research has shown that this protein is also expressed in the female rat.[78] This protein binds pheromones released from the urine of males and affects the sexual behavior of female mice. Therefore, the high level of Mup1 protein in protein coronas of male samples compared with those of female coronas is in line with the literature[78] and can be a validation of our approach. Some of the significant proteins identified in Stöber 100 NP coronas might also have diagnostic potential. For instance, Krt16, which acts as a regulator of innate immunity in response to skin barrier breach, is a target of an autoantibody response in complex regional pain syndrome and TFAP2A-induced Krt16 overexpression promotes tumorigenicity in lung adenocarcinoma in mice.[79] The higher abundance of a specific protein in male vs female does not always correlate to the enrichment in the corona, as the binding kinetics may be affected by the presence of other proteins (due to protein−protein interactions and surface accessibility). In principle, protein "X" may have the same concentration in female and male but it could be differentially enriched in the corona due to the presence/absence of other proteins that are specific to each sex.

Finally, comparing protein abundances between male and female protein coronas of Stöber 50 NPs demonstrated that four proteins had a *P* value <0.05 with higher corona concentration in male coronas (Rab27b, Ig heavy-chain V region 5−84, H4c1 and Ig heavy-chain V region MOPC 173) (Table 2). Ig heavy-chain V region MOPC 173 was also found at a significantly higher concentration in the female coronas of Stöber 100 NP coronas. Rab27b is a secretory protein and in humans, has been indicated as a potential marker of breast cancer progression,[80,81] and an independent prognostic marker for pancreatic ductal adenocarcinoma,[82] as well as other cancers.

Figure 7 shows the Venn diagrams of the identified proteins on male and female protein coronas for the three silica NPs with distinct physicochemical properties. The results demonstrate that the protein corona formation depends on the size

https://doi.org/10.1021/acsbiomedchemau.2c00040
ACS Bio Med Chem Au 2023, 3, 62−73

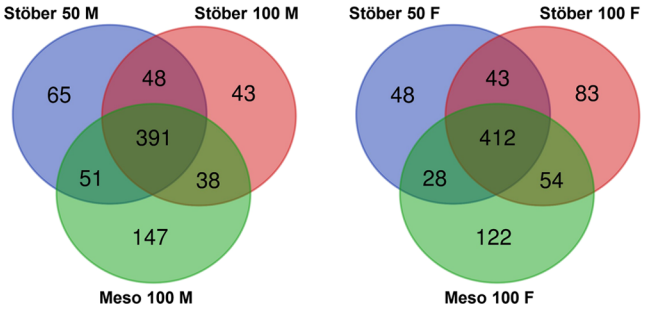

Figure 7. Venn charts showing the effect of size and porosity on the numbers of identified proteins in the male and female protein corona profiles. Venn diagram analysis reveals that the protein corona formation depends on the size and porosity of the structure in male and female protein coronas (the number of unique proteins varies in different NPs).

and porosity of the structure in male and female protein coronas. By increasing porosity (i.e., Stöber vs mesoporous particles), the numbers of unique proteins increase, which may be due to the higher active surface area of mesoporous 100 NPs, compared to Stöber NPs, that are available for the adsorption of the proteins. As almost all of the identified sex-specific significant proteins in the corona profiles, regardless of the size and porosity of the employed silica NPs, had a higher contribution in male coronas, our results suggest that the diagnostic capacity of these tested silica NPs may be stronger for males than for females.

The open targets platform (https://platform.opentargets.org) is a tool for scoring target-disease associations in humans.[83] RETN is the human version of mouse Retn that was picked up by our analysis of mesoporous 100 NP coronas. Quering RETN in open targets platform showed the association of this protein with insulin resistance, rheumatoid arthritis, diabetes, and coronary artery disease as the top hits. Therefore, similar studies using differential adsorption of human protein coronas will have implications for the utility of silica NPs for diagnostic and therapeutic applications.

CONCLUSIONS

In this study, we investigated the influence of the plasma sex-dependent composition of protein corona at the surface of three silica NPs with distinct physicochemical properties. Our proof-of-concept results revealed that, after incubation of mesoporous (100 nm) and Stöber (100 and 50 nm) silica nanoparticles with plasma proteins of female and male BALB/c mice, the protein corona composition was sex-specific: 17, 4, and 4 distinct sex-specific proteins were detected for mesoporous silica NPs and Stöber silica nanoparticles of ~100, 50, and 100 nm in diameter, respectively. The identified sex disparities in protein corona profiles of NPs in this study will enable the researchers to use informed strategies to compensate for the effect of sex disparities on the diagnostic and therapeutic efficacies of NPs. For example, adjusting the dosage of nanotherapeutics (e.g., in nano-based vaccines) can improve the therapeutic benefits of NPs in both sexes.[8,37] Thus, the outcomes from this proof-of-concept study (of course in combination with future sex-specific studies on the protein corona of various NPs) could create a significant impact on the development of more effective and safer sex-specific nanomedicine diagnostics and therapeutics.

ASSOCIATED CONTENT

Supporting Information

The Supporting Information is available free of charge at https://pubs.acs.org/doi/10.1021/acsbiomedchemau.2c00040.

TEM images of NPs coated with female plasma protein (Figure S1) (PDF)

The LC-MS/MS outcomes of the male and female protein coronas at the surface of various NPs together with the male and female whole plasma analysis resulted in identification of 1690 proteins (Table S1) (XLSX)

A list of proteins in each cluster (Table S2) (XLSX)

A total of 25 proteins were identified with significant differences in male vs female protein corona profiles of the three NP types (Table S3) (XLSX)

AUTHOR INFORMATION

Corresponding Authors

Amir Ata Saei − *Division of Physiological Chemistry I, Department of Medical Biochemistry and Biophysics, Karolinska Institute, SE-17 165 Stockholm, Sweden;* orcid.org/0000-0002-2639-6328; Email: amirata.saei.dibavar@ki.se

Morteza Mahmoudi − *Department of Radiology and Precision Health Program, Michigan State University, East Lansing, Michigan 48824, United States; Mary Horrigan Connors Center for Women's Health and Gender Biology, Brigham and Women's Hospital, Harvard Medical School, Boston, Massachusetts 02115, United States;* orcid.org/0000-0002-2575-9684; Email: mahmou22@msu.edu

Authors

Ali Akbar Ashkarran − *Department of Radiology and Precision Health Program, Michigan State University, East Lansing, Michigan 48824, United States*

Hassan Gharibi − *Division of Physiological Chemistry I, Department of Medical Biochemistry and Biophysics, Karolinska Institute, SE-17 165 Stockholm, Sweden;* orcid.org/0000-0002-3072-4929

Jason W. Grunberger − *Utah Center for Nanomedicine, University of Utah, Salt Lake City, Utah 84112, United States*

Nitish Khurana − *Utah Center for Nanomedicine, University of Utah, Salt Lake City, Utah 84112, United States*

Raziye Mohammadpour − *Utah Center for Nanomedicine, University of Utah, Salt Lake City, Utah 84112, United States*

Hamidreza Ghandehari − *Utah Center for Nanomedicine, University of Utah, Salt Lake City, Utah 84112, United States; Department of Biomedical Engineering, University of Utah, Salt Lake City, Utah 84112, United States;* orcid.org/0000-0002-9333-9964

Complete contact information is available at: https://pubs.acs.org/10.1021/acsbiomedchemau.2c00040

Author Contributions

○A.A.A. and H. Gharibi contributed equally.

Author Contributions

CRediT: **Ali Akbar Ashkarran** data curation (equal), formal analysis (equal), investigation (equal), methodology (equal),

https://doi.org/10.1021/acsbiomedchemau.2c00040
ACS Bio Med Chem Au 2023, 3, 62−73

validation (equal), visualization (equal), writing-original draft (equal), writing-review & editing (equal); **Hassan Gharibi** data curation (equal), formal analysis (equal), validation (equal), visualization (equal), writing-original draft (equal); **Jason W Grunberger** investigation (equal), methodology (equal), writing-original draft (equal), writing-review & editing (equal); **Amir Ata Saei** data curation (equal), formal analysis (equal), investigation (equal), validation (equal), visualization (equal), writing-original draft (equal), writing-review & editing (equal); **Nitish Khurana** methodology (equal), writing-original draft (equal); **Raziye Mohammadpour** investigation (equal), methodology (equal); **Hamidreza Ghandehari** conceptualization (equal), resources (equal), supervision (equal), validation (equal), writing-review & editing (equal); **Morteza Mahmoudi** conceptualization (equal), funding acquisition (equal), resources (equal), supervision (equal), writing-review & editing (equal).

Notes

The authors declare the following competing financial interest(s): Morteza Mahmoudi discloses that (i) he is a co-founder and director of the Academic Parity Movement (www.paritymovement.org), a non-profit organization dedicated to addressing academic discrimination, violence and incivility; (ii) he is a Founding Partner at Partners in Global Wound Care (PGWC); and (iii) he receives royalties/honoraria for his published books, plenary lectures, and licensed patent.

■ ACKNOWLEDGMENTS

This work was supported by the U.S. National Institute of Diabetes and Digestive and Kidney Diseases (Grant DK131417-01) and the U.S. National Institute of Environmental Health Sciences (R01ES024681). A.A.S. was supported by the Swedish Research Council (Grant 2020-00687). M.M. acknowledges Mary Horrigan Connors Center for Women's Health and Gender Biology, Brigham and Women's Hospital, Harvard Medical School for IGNITE award.

■ REFERENCES

(1) Wilhelm, S.; Tavares, A. J.; Dai, Q.; Ohta, S.; Audet, J.; Dvorak, H. F.; Chan, W. C. Analysis of nanoparticle delivery to tumours. *Nat. Rev. Mater.* **2016**, *1*, 16014.
(2) Park, K. The beginning of the end of the nanomedicine hype. *J. Controlled Release* **2019**, *305*, 221−222.
(3) Sun, A.; Benet, L. Z. Late-Stage Failures of Monoclonal Antibody Drugs: A Retrospective Case Study Analysis. *Pharmacology* **2020**, *105*, 145−163.
(4) Mahmoudi, M. The need for robust characterization of nanomaterials for nanomedicine applications. *Nat. Commun.* **2021**, *12*, No. 5246.
(5) Mahmoudi, M. The need for improved methodology in protein corona analysis. *Nat. Commun.* **2022**, *13*, No. 49.
(6) Ashkarran, A. A.; Swann, J.; Hollis, L.; Mahmoudi, M. The File Drawer Problem in Nanomedicine. *Trends Biotechnol.* **2021**, *39*, 425−427.
(7) Derakhshi, M.; Daemi, S.; Shahini, P.; Habibzadeh, A.; Mostafavi, E.; Ashkarran, A. A. Two-Dimensional Nanomaterials beyond Graphene for Biomedical Applications. *J. Funct. Biomater.* **2022**, *13*, No. 27.
(8) Hajipour, M. J.; Aghaverdi, H.; Serpooshan, V.; Vali, H.; Sheibani, S.; Mahmoudi, M. Sex as an important factor in nanomedicine. *Nat. Commun.* **2021**, *12*, No. 2984.
(9) Arnold, A. P.; Disteche, C. M. Sexual Inequality in the Cancer Cell. *Cancer Res.* **2018**, *78*, 5504−5505.
(10) Li, C. H.; Haider, S.; Shiah, Y.-J.; Thai, K.; Boutros, P. C. Sex Differences in Cancer Driver Genes and Biomarkers. *Cancer Res.* **2018**, *78*, 5527−5537.
(11) Lopes-Ramos, C. M.; Kuijjer, M. L.; Ogino, S.; Fuchs, C. S.; DeMeo, D. L.; Glass, K.; Quackenbush, J. Gene Regulatory Network Analysis Identifies Sex-Linked Differences in Colon Cancer Drug Metabolism. *Cancer Res.* **2018**, *78*, 5538−5547.
(12) Chaligné, R.; Heard, E. X-chromosome inactivation in development and cancer. *FEBS Lett.* **2014**, *588*, 2514−2522.
(13) Dunford, A.; Weinstock, D. M.; Savova, V.; Schumacher, S. E.; Cleary, J. P.; Yoda, A.; Sullivan, T. J.; Hess, J. M.; Gimelbrant, A. A.; Beroukhim, R.; et al. Tumor-suppressor genes that escape from X-inactivation contribute to cancer sex bias. *Nat. Genet.* **2017**, *49*, 10.
(14) Donington, J. S.; Colson, Y. L. Sex and Gender Differences in Non-Small Cell Lung Cancer. In *Seminars in Thoracic and Cardiovascular Surgery*; Elsevier, 2011; pp 137−145.
(15) Carey, M. A.; Card, J. W.; Voltz, J. W.; Arbes, S. J., Jr; Germolec, D. R.; Korach, K. S.; Zeldin, D. C. It's all about sex: gender, lung development and lung disease. *Trends Endocrinol. Metab.* **2007**, *18*, 308−313.
(16) Siegel, R. L.; Miller, K.; Jemal, A. Cancer Statistics, 2017. *CA: Cancer J. Clin.* **2017**, *67*, 7−30.
(17) Kabir, Z.; Connolly, G. N.; Clancy, L. Sex-differences in lung cancer cell-types? An epidemiologic study in Ireland. *Ulster Med. J.* **2008**, *77*, 31.
(18) Poley, M.; Chen, G.; Sharf-Pauker, N.; Avital, A.; Kaduri, M.; Sela, M.; Raimundo, P. M.; Koren, L.; Arber, S.; Egorov, E.; Shainsky, J.; Shklover, J.; Schroeder, A. Sex-Based Differences in the Biodistribution of Nanoparticles and Their Effect on Hormonal, Immune, and Metabolic Function. *Advanced NanoBiomed Research* **2022**.
(19) James, B. D.; Guerin, P.; Allen, J. B. Let's Talk About Sex—Biological Sex Is Underreported in Biomaterial Studies. *Adv. Healthcare Mater.* **2021**, *10*, No. 2001034.
(20) Serpooshan, V.; Sheibani, S.; Pushparaj, P.; Wojcik, M.; Jang, A. Y.; Santoso, M. R.; Jang, J. H.; Huang, H.; Safavi-Sohi, R.; Haghjoo, N.; Nejadnik, H.; Aghaverdi, H.; Vali, H.; Kinsella, J. M.; Presley, J.; Xu, K.; Yang, P. C. M.; Mahmoudi, M. Effect of Cell Sex on Uptake of Nanoparticles: The Overlooked Factor at the Nanobio Interface. *ACS Nano* **2018**, *12*, 2253−2266.
(21) Monopoli, M. P.; Åberg, C.; Salvati, A.; Dawson, K. A. Biomolecular coronas provide the biological identity of nanosized materials. *Nat. Nanotechnol.* **2012**, *7*, 779−786.
(22) Ashkarran, A. A.; Dararatana, N.; Crespy, D.; Caracciolo, G.; Mahmoudi, M. Mapping the heterogeneity of protein corona by: Ex vivo magnetic levitation. *Nanoscale* **2020**, *12*, 2374−2383.
(23) Mahmoudi, M. Debugging nano−bio interfaces: systematic strategies to accelerate clinical translation of nanotechnologies. *Trends Biotechnol.* **2018**, *36*, 755−769.
(24) Mahmoudi, M.; Yu, M.; Serpooshan, V.; Wu, J. C.; Langer, R.; Lee, R. T.; Karp, J. M.; Farokhzad, O. C. Multiscale technologies for treatment of ischemic cardiomyopathy. *Nat. Nanotechnol.* **2017**, *12*, 845.
(25) Hajipour, M. J.; Mehrani, M.; Abbasi, S. H.; Amin, A.; Kassaian, S. E.; Garbern, J. C.; Caracciolo, G.; Zanganeh, S.; Chitsazan, M.; Aghaverdi, H.; Kamali Shahri, S. M.; Ashkarran, A.; Raoufi, M.; Bauser-Heaton, H.; Zhang, J.; Muehlschlegel, J. D.; Moore, A.; Lee, R. T.; Wu, J. C.; Serpooshan, V.; Mahmoudi, M. Nanoscale Technologies for Prevention and Treatment of Heart Failure: Challenges and Opportunities. *Chem. Rev.* **2019**, *119*, 11352−11390.
(26) Mahmoudi, M.; Lynch, I.; Ejtehadi, M. R.; Monopoli, M. P.; Bombelli, F. B.; Laurent, S. Protein− nanoparticle interactions: opportunities and challenges. *Chem. Rev.* **2011**, *111*, 5610−5637.
(27) Heydari, T.; Heidari, M.; Mashinchian, O.; Wojcik, M.; Xu, K.; Dalby, M. J.; Mahmoudi, M.; Ejtehadi, M. R. Development of a Virtual Cell Model to Predict Cell Response to Substrate Topography. *ACS Nano* **2017**, *11*, 9084−9092.
(28) Silliman, C. C.; Dzieciatkowska, M.; Moore, E. E.; Kelher, M. R.; Banerjee, A.; Liang, X.; Land, K. J.; Hansen, K. C. Proteomic

analyses of human plasma: Venus versus Mars. *Transfusion* **2012**, *52*, 417−424.
(29) Krumsiek, J.; Mittelstrass, K.; Do, K. T.; Stückler, F.; Ried, J.; Adamski, J.; Peters, A.; Illig, T.; Kronenberg, F.; Friedrich, N.; et al. Gender-specific pathway differences in the human serum metabolome. *Metabolomics* **2015**, *11*, 1815−1833.
(30) Caracciolo, G.; Safavi-Sohi, R.; Malekzadeh, R.; Poustchi, H.; Vasighi, M.; Zenezini Chiozzi, R.; Capriotti, A. L.; Laganà, A.; Hajipour, M.; Di Domenico, M.; Di Carlo, A.; Caputo, D.; Aghaverdi, H.; Papi, M.; Palmieri, V.; Santoni, A.; Palchetti, S.; Digiacomo, L.; Pozzi, D.; Suslick, K. S.; Mahmoudi, M. Disease-specific protein corona sensor arrays may have disease detection capacity. *Nanoscale Horiz.* **2019**, *4*, 1063−1076.
(31) Hajipour, M. J.; Laurent, S.; Aghaie, A.; Rezaee, F.; Mahmoudi, M. Personalized protein coronas: a "key" factor at the nanobiointerface. *Biomater. Sci.* **2014**, *2*, 1210−1221.
(32) Tavakol, M.; Montazeri, A.; Naghdabadi, R.; Hajipour, M. J.; Zanganeh, S.; Caracciolo, G.; Mahmoudi, M. Disease-related metabolites affect protein−nanoparticle interactions. *Nanoscale* **2018**, *10*, 7108−7115.
(33) Vignoli, A.; Tenori, L.; Luchinat, C.; Saccenti, E. Age and Sex Effects on Plasma Metabolite Association Networks in Healthy Subjects. *J. Proteome Res.* **2018**, *17*, 97−107.
(34) Krumsiek, J.; Mittelstrass, K.; Do, K. T.; Stückler, F.; Ried, J.; Adamski, J.; Peters, A.; Illig, T.; Kronenberg, F.; Friedrich, N.; Nauck, M.; Pietzner, M.; Mook-Kanamori, D. O.; Suhre, K.; Gieger, C.; Grallert, H.; Theis, F. J.; Kastenmüller, G. Gender-specific pathway differences in the human serum metabolome. *Metabolomics* **2015**, *11*, 1815−1833.
(35) Hajipour, M. J.; Aghaverdi, H.; Serpooshan, V.; Vali, H.; Sheibani, S.; Mahmoudi, M. Sex as an important factor in nanomedicine. *Nat. Commun.* **2021**, *12*, No. 2984.
(36) Ashkarran, A. A.; Ghavami, M.; Aghaverdi, H.; Stroeve, P.; Mahmoudi, M. Bacterial effects and protein corona evaluations: Crucial ignored factors in the prediction of bio-efficacy of various forms of silver nanoparticles. *Chem. Res. Toxicol.* **2012**, *25*, 1231−1242.
(37) Vulpis, E.; Giulimondi, F.; Digiacomo, L.; Zingoni, A.; Safavi-Sohi, R.; Sharifi, S.; Caracciolo, G.; Mahmoudi, M. The Possible Role of Sex As an Important Factor in Development and Administration of Lipid Nanomedicine-Based COVID-19 Vaccine. *Mol. Pharmaceutics* **2021**, *18*, 2448−2453.
(38) Panáček, A.; Kvítek, L.; Smékalová, M.; Večeřová, R.; Kolář, M.; Röderová, M.; Dyčka, F.; Šebela, M.; Prucek, R.; Tomanec, O.; Zbořil, R. Bacterial resistance to silver nanoparticles and how to overcome it. *Nat. Nanotechnol.* **2018**, *13*, 65−71.
(39) Mohammadpour, R.; Cheney, D. L.; Grunberger, J. W.; Yazdimamaghani, M.; Jedrzkiewicz, J.; Isaacson, K. J.; Dobrovolskaia, M. A.; Ghandehari, H. One-year chronic toxicity evaluation of single dose intravenously administered silica nanoparticles in mice and their Ex vivo human hemocompatibility. *J. Controlled Release* **2020**, *324*, 471−481.
(40) Mohammadpour, R.; Dobrovolskaia, M. A.; Cheney, D. L.; Greish, K. F.; Ghandehari, H. Subchronic and chronic toxicity evaluation of inorganic nanoparticles for delivery applications. *Adv. Drug Delivery Rev.* **2019**, *144*, 112−132.
(41) Mohammadpour, R.; Yazdimamaghani, M.; Cheney, D. L.; Jedrzkiewicz, J.; Ghandehari, H. Subchronic toxicity of silica nanoparticles as a function of size and porosity. *J. Controlled Release* **2019**, *304*, 216−232.
(42) Chen, Y.; Chen, H.; Shi, J. In vivo bio-safety evaluations and diagnostic/therapeutic applications of chemically designed mesoporous silica nanoparticles. *Adv. Mater.* **2013**, *25*, 3144−3176.
(43) Jafari, S.; Derakhshankhah, H.; Alaei, L.; Fattahi, A.; Varnamkhasti, B. S.; Saboury, A. A. Mesoporous silica nanoparticles for therapeutic/diagnostic applications. *Biomed. Pharmacother.* **2019**, *109*, 1100−1111.
(44) Janjua, T. I.; Cao, Y.; Yu, C.; Popat, A. Clinical translation of silica nanoparticles. *Nat. Rev. Mater.* **2021**, *6*, 1072−1074.
(45) Vallet-Regí, M.; Colilla, M.; Izquierdo-Barba, I.; Manzano, M. Mesoporous silica nanoparticles for drug delivery: Current insights. *Molecules* **2018**, *23*, 47.
(46) Mamaeva, V.; Sahlgren, C.; Lindén, M. Mesoporous silica nanoparticles in medicine—Recent advances. *Adv. Drug Delivery Rev.* **2013**, *65*, 689−702.
(47) Lesniak, A.; Fenaroli, F.; Monopoli, M. P.; Åberg, C.; Dawson, K. A.; Salvati, A. Effects of the presence or absence of a protein corona on silica nanoparticle uptake and impact on cells. *ACS Nano* **2012**, *6*, 5845−5857.
(48) Tenzer, S.; Docter, D.; Kuharev, J.; Musyanovych, A.; Fetz, V.; Hecht, R.; Schlenk, F.; Fischer, D.; Kiouptsi, K.; Reinhardt, C.; et al. Rapid formation of plasma protein corona critically affects nanoparticle pathophysiology. *Nat. Nanotechnol.* **2013**, *8*, 772−781.
(49) Monopoli, M. P.; Walczyk, D.; Campbell, A.; Elia, G.; Lynch, I.; Baldelli Bombelli, F.; Dawson, K. A. Physical− chemical aspects of protein corona: relevance to in vitro and in vivo biological impacts of nanoparticles. *J. Am. Chem. Soc.* **2011**, *133*, 2525−2534.
(50) Walczyk, D.; Bombelli, F. B.; Monopoli, M. P.; Lynch, I.; Dawson, K. A. What the cell "sees" in bionanoscience. *J. Am. Chem. Soc.* **2010**, *132*, 5761−5768.
(51) Salvati, A.; Pitek, A. S.; Monopoli, M. P.; Prapainop, K.; Bombelli, F. B.; Hristov, D. R.; Kelly, P. M.; Åberg, C.; Mahon, E.; Dawson, K. A. Transferrin-functionalized nanoparticles lose their targeting capabilities when a biomolecule corona adsorbs on the surface. *Nat. Nanotechnol.* **2013**, *8*, 137−143.
(52) Sheibani, S.; Basu, K.; Farnudi, A.; Ashkarran, A.; Ichikawa, M.; Presley, J. F.; Bui, K. H.; Ejtehadi, M. R.; Vali, H.; Mahmoudi, M. Nanoscale characterization of the biomolecular corona by cryo-electron microscopy, cryo-electron tomography, and image simulation. *Nat. Commun.* **2021**, *12*, No. 573.
(53) Blume, J. E.; Manning, W. C.; Troiano, G.; Hornburg, D.; Figa, M.; Hesterberg, L.; Platt, T. L.; Zhao, X.; Cuaresma, R. A.; Everley, P. A.; Ko, M.; Liou, H.; Mahoney, M.; Ferdosi, S.; Elgierari, E. M.; Stolarczyk, C.; Tangeysh, B.; Xia, H.; Benz, R.; Siddiqui, A.; Carr, S. A.; Ma, P.; Langer, R.; Farias, V.; Farokhzad, O. C. Rapid, deep and precise profiling of the plasma proteome with multi-nanoparticle protein corona. *Nat. Commun.* **2020**, *11*, No. 3662.
(54) Caracciolo, G.; Safavi-Sohi, R.; Malekzadeh, R.; Poustchi, H.; Vasighi, M.; Chiozzi, R. Z.; Capriotti, A. L.; Laganà, A.; Hajipour, M.; Di Domenico, M.; Di Carlo, A.; Caputo, D.; Aghaverdi, H.; Papi, M.; Palmieri, V.; Santoni, A.; Palchetti, S.; Digiacomo, L.; Pozzi, D.; Suslick, K. S.; Mahmoudi, M. Disease-specific protein corona sensor arrays may have disease detection capacity. *Nanoscale Horiz.* **2019**, *4*, 1063−1076.
(55) Geyer, P. E.; Holdt, L. M.; Teupser, D.; Mann, M. Revisiting biomarker discovery by plasma proteomics. *Mol. Syst. Biol.* **2017**, *13*, 942.
(56) Keshishian, H.; Burgess, M. W.; Specht, H.; Wallace, L.; Clauser, K. R.; Gillette, M. A.; Carr, S. A. Quantitative, multiplexed workflow for deep analysis of human blood plasma and biomarker discovery by mass spectrometry. *Nat. Protoc.* **2017**, *12*, 1683−1701.
(57) Jamaluddin, M. S; Weakley, S. M; Yao, Q.; Chen, C. Resistin: functional roles and therapeutic considerations for cardiovascular disease. *British journal of pharmacology* **2012**, *165*, 622−63.
(58) Rak, A.; Mellouk, N.; Froment, P.; Dupont, J. Adiponectin and resistin: Potential metabolic signals affecting hypothalamo-pituitary gonadal axis in females and males of different species. *Reproduction* **2017**, *153*, R215−R226.
(59) Small, H. Y.; McNeilly, S.; Mary, S.; Sheikh, A. M.; Delles, C. Resistin Mediates Sex-Dependent Effects of Perivascular Adipose Tissue on Vascular Function in the Shrsp. *Sci. Rep.* **2019**, *9*, No. 6897.
(60) Ribot, J.; Rodríguez, A. M.; Rodríguez, E.; Palou, A. Adiponectin and resistin response in the onset of obesity in male and female rats. *Obesity* **2008**, *16*, 723−730.
(61) Konrad, A.; Lehrke, M.; Schachinger, V.; Seibold, F.; Stark, R.; Ochsenkühn, T.; Parhofer, K. G.; Göke, B.; Broedl, U. C. Resistin is an inflammatory marker of inflammatory bowel disease in humans. *Eur. J. Gastroenterol. Hepatol.* **2007**, *19*, 1070−1074.

https://doi.org/10.1021/acsbiomedchemau.2c00040
ACS Bio Med Chem Au 2023, 3, 62−73

(62) Danese, E.; Montagnana, M.; Minicozzi, A. M.; Bonafini, S.; Ruzzenente, O.; Gelati, M.; De Manzoni, G.; Lippi, G.; Guidi, G. C. The role of resistin in colorectal cancer. *Clin. Chim. Acta* **2012**, *413*, 760−764.
(63) Reilly, M. P.; Lehrke, M.; Wolfe, M. L.; Rohatgi, A.; Lazar, M. A.; Rader, D. J. Resistin is an inflammatory marker of atherosclerosis in humans. *Circulation* **2005**, *111*, 932−939.
(64) de León, A. C.; González, D. A.; Hernández, A. G.; Sánchez, J. J. A.; Díaz, B. B.; Coello, S. D.; Rodríguez, I. M.; García, J. G. O.; Jaime, A. A.; Pérez, M. C. R. The association of resistin with coronary disease in the general population. *J. Atheroscler. Thromb.* **2014**, *21*, 273−281.
(65) Ellington, A. A.; Malik, A. R.; Klee, G. G.; Turner, S. T.; Rule, A. D.; Mosley, T. H., Jr.; Kullo, I. J. Association of plasma resistin with glomerular filtration rate and albuminuria in hypertensive adults. *Hypertension* **2007**, *50*, 708−714.
(66) Yoshino, T.; Kusunoki, N.; Tanaka, N.; Kaneko, K.; Kusunoki, Y.; Endo, H.; Hasunuma, T.; Kawai, S. Elevated serum levels of resistin, leptin, and adiponectin are associated with c-reactive protein and also other clinical conditions in rheumatoid arthritis. *Intern. Med.* **2011**, *50*, 269−275.
(67) Cui, R.; Wang, C.; Zhao, Q.; Wang, Y.; Li, Y. Serum carboxypeptidase N1 serves as a potential biomarker complementing ca15-3 for breast cancer. *Anti-Cancer Agents Med. Chem.* **2020**, *20*, 2053−2065.
(68) Cai, Y.; Wu, D.; Zhan, L. CCT6A expression in hepatocellular carcinoma and its correlation with clinical characteristics, liver function indexes, tumor markers and prognosis. *Clin. Res. Hepatol. Gastroenterol.* **2022**, *46*, No. 101796.
(69) Beker, B. M.; Corleto, M. G.; Fieiras, C.; Musso, C. G. Novel acute kidney injury biomarkers: their characteristics, utility and concerns. *Int. Urol. Nephrol.* **2018**, *50*, 705−713.
(70) Gombart, A. F.; Bhan, I.; Borregaard, N.; Tamez, H.; Camargo, C. A., Jr; Koeffler, H. P.; Thadhani, R. Low plasma level of cathelicidin antimicrobial peptide (hCAP18) predicts increased infectious disease mortality in patients undergoing hemodialysis. *Clin. Infect. Dis.* **2009**, *48*, 418−424.
(71) Lubbers, R.; van Essen, M. F.; van Kooten, C.; Trouw, L. A. Production of complement components by cells of the immune system. *Clin. Exp. Immunol.* **2017**, *188*, 183−194.
(72) da Costa, M. G.; Poppelaars, F.; Van Kooten, C.; Mollnes, T. E.; Tedesco, F.; Würzner, R.; Trouw, L. A.; Truedsson, L.; Daha, M. R.; Roos, A.; Seelen, M. A. Age and sex-associated changes of complement activity and complement levels in a healthy caucasian population. *Front. Immunol.* **2018**, *9*, No. 2664.
(73) Hajishengallis, G.; Reis, E. S.; Mastellos, D. C.; Ricklin, D.; Lambris, J. D. Novel mechanisms and functions of complement. *Nat. Immunol.* **2017**, *18*, 1288−1298.
(74) Cao, L.; Cobbs, A.; Simon, R. P.; Zhou, A. Distinct plasma proteomic changes in male and female African American stroke patients. *Int. J. Physiol., Pathophysiol. Pharmacol.* **2019**, *11*, 12−20.
(75) Smith-Bouvier, D. L.; Divekar, A. A.; Sasidhar, M.; Du, S.; Tiwari-Woodruff, S. K.; King, J. K.; Arnold, A. P.; Singh, R. R.; Voskuhl, R. R. A role for sex chromosome complement in the female bias in autoimmune disease. *J. Exp. Med.* **2008**, *205*, 1099−1108.
(76) Wang, D. J.; Zhi, X. Y.; Zhang, S. C.; Jiang, M.; Liu, P.; Han, X. P.; Li, J.; Chen, Z.; Wang, C. L. The bone morphogenetic protein antagonist gremlin is overexpressed in human malignant mesothelioma. *Oncol. Rep.* **2012**, *27*, 58−64.
(77) Chang, Y. T.; Tsai, W. C.; Lin, W. Z.; Wu, C. C.; Yu, J. C.; Tseng, V. S.; Liao, G. S.; Hu, J. M.; Hsu, H. M.; Chang, Y. J.; Lin, M. C.; Chu, C. M.; Yang, C. Y.; Novel, A. IGLC2 Gene Linked With Prognosis of Triple-Negative Breast Cancer. *Front. Oncol.* **2022**, *11*, No. 759952.
(78) Kondo, Y.; Yamada, J. Male urinary protein-1 (Mup-1) expression in the female rat. *J. Heredity* **1983**, *74*, 280−282.
(79) Yuanhua, L.; Pudong, Q.; Wei, Z.; Yuan, W.; Delin, L.; Yan, Z.; Geyu, L.; Bo, S. TFAP2A induced KRT16 as an oncogene in lung adenocarcinoma via EMT. *Int. J. Biol. Sci.* **2019**, *15*, 1419−1428.
(80) Hendrix, A.; Braems, G.; Bracke, M.; Seabra, M.; Gahl, W.; De Wever, O.; Westbroek, W. The secretory small GTPase Rab27B as a marker for breast cancer progression. *Oncotarget* **2010**, *1*, 304−308.
(81) Zhang, J. X.; Huang, X. X.; Cai, M. B.; Tong, Z. T.; Chen, J. W.; Qian, D.; Liao, Y. J.; Deng, H. X.; Liao, D. Z.; Huang, M. Y.; Zeng, Y. X.; Xie, D.; Mai, S. J. Overexpression of the secretory small GTPase Rab27B in human breast cancer correlates closely with lymph node metastasis and predicts poor prognosis. *J. Transl. Med.* **2012**, *10*, No. 242.
(82) Zhao, H.; Wang, Q.; Wang, X.; Zhu, H.; Zhang, S.; Wang, W.; Wang, Z.; Huang, J. Correlation between RAB27B and p53 Expression and Overall Survival in Pancreatic Cancer. *Pancreas* **2016**, *45*, 204−210.
(83) Ochoa, D.; Hercules, A.; Carmona, M.; Suveges, D.; Gonzalez-Uriarte, A.; Malangone, C.; Miranda, A.; Fumis, L.; Carvalho-Silva, D.; Spitzer, M.; et al. Open Targets Platform: supporting systematic drug−target identification and prioritisation. *Nucleic Acids Res.* **2021**, *49*, D1302−D1310.

https://doi.org/10.1021/acsbiomedchemau.2c00040
ACS Bio Med Chem Au 2023, 3, 62−73